JACS
JOURNAL OF THE AMERICAN CHEMICAL SOCIETY
Article
pubs.acs.org/JACS

Understanding Interactions between Manganese Oxide and Gold That Lead to Enhanced Activity for Electrocatalytic Water Oxidation

Yelena Gorlin,[†] Chia-Jung Chung,[‡] Jesse D. Benck,[†] Dennis Nordlund,[§] Linsey Seitz,[†] Tsu-Chien Weng,[§] Dimosthenis Sokaras,[§] Bruce M. Clemens,[‡] and Thomas F. Jaramillo*[,†]

[†]Department of Chemical Engineering, [‡]Department of Materials Science and Engineering, Stanford University, Stanford, California 94305, United States

[§]SLAC National Accelerator Laboratory, 2575 Sand Hill Road, Menlo Park, California 94025, United States

Supporting Information

ABSTRACT: To develop active nonprecious metal-based electrocatalysts for the oxygen evolution reaction (OER), a limiting reaction in several emerging renewable energy technologies, a deeper understanding of the activity of the first row transition metal oxides is needed. Previous studies of these catalysts have reported conflicting results on the influence of noble metal supports on the OER activity of the transition metal oxides. Our study aims to clarify the interactions between a transition metal oxide catalyst and its metal support in turning over this reaction. To achieve this goal, we examine a catalytic system comprising nanoparticulate Au, a common electrocatalytic support, and nanoparticulate MnO_x, a promising OER catalyst. We conclusively demonstrate that adding Au to MnO_x significantly enhances OER activity relative to MnO_x in the absence of Au, producing an order of magnitude higher turnover frequency (TOF) than the TOF of the best pure MnO_x catalysts reported to date. We also provide evidence that it is a local rather than bulk interaction between Au and MnO_x that leads to the observed enhancement in the OER activity. Engineering improvements in nonprecious metal-based catalysts by the addition of Au or other noble metals could still represent a scalable catalyst as even trace amounts of Au are shown to lead a significant enhancement in the OER activity of MnO_x.

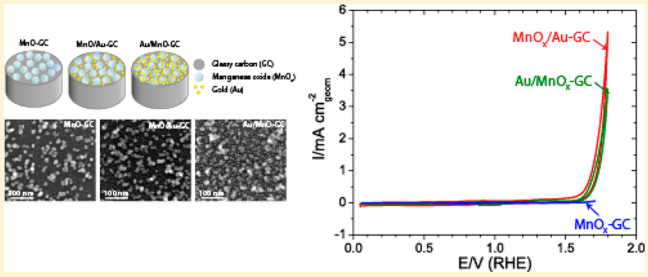

INTRODUCTION

Electrochemical water oxidation, also known as the oxygen evolution reaction (OER), is a key energy conversion reaction in a number of clean energy technologies, including rechargeable metal−air batteries, electrolysis cells, and solar fuel production.[1,2] Widespread commercialization of these technologies is limited in part by the scarcity and high cost of the best known catalysts for the OER, ruthenium and iridium oxides.[3,4] Nickel oxides (NiO_x) present a viable alternative to precious metal oxides in alkaline environments and are currently used in commercially available alkaline electrolyzers.[3,5] Other nonprecious metal oxides, including manganese oxides (MnO_x) and cobalt oxides (CoO_x), have also demonstrated promising OER activity under alkaline conditions.[4,6−19] To facilitate the development of nonprecious metal OER catalysts with improved activities, it is necessary to identify the specific catalytic sites that participate in the reaction and accurately determine their turnover frequencies. Although isolating site-specific turnover frequencies can be challenging in oxide electrocatalysts, the likelihood of success can be improved if the catalytic activity is studied on well-defined materials deposited on inert supports.[20]

There have been conflicting reports in the recent literature regarding the role metal supports play in the OER activity of metal oxide catalysts. A study, which used Pt(111) and Au(111) single crystal surfaces as supports for OER catalysts, demonstrated that the OER activity of four first row transitional metal oxides did not vary with the nature of the metal support and was linearly dependent on the coverage of the support by the metal oxide.[6] Other reports, however, have shown that the OER activities of nickel,[21] cobalt,[17] and manganese oxides[22,23] were influenced by the nature of the underlying support, and that the OER turnover frequency of a bulk metal oxide was inferior to that of a submonolayer amount of the same metal oxide deposited on a metal support.[17,21] Our study, which focuses on one particular metal−supported transition metal oxide system, MnO_x/Au, conclusively demonstrates that adding a noble metal to a metal oxide OER catalyst can have a significant impact on its electrocatalytic activity. We show that this impact cannot be explained simply by surface area effects and we identify interesting changes in the red-ox properties of both MnO_x and Au when the two materials are present in one composite catalyst. Using our experimental data and previous literature results, we develop a hypothesis about potential OER active sites.

Received: July 23, 2013
Published: March 24, 2014

   dx.doi.org/10.1021/ja407581w | J. Am. Chem. Soc. 2014, 136, 4920−4926

EXPERIMENTAL SECTION

Preparation of rotating disk electrode substrates: Rotating disk electrode substrates were prepared from 200 mm long glassy carbon (GC) rods (diameter 5 mm, Sigradur G HTW Hochtemperatur-Werkstoffe GmbH). Before deposition of MnO or Au nanoparticles, the rods were processed by Stanford crystal shop to produce 4 mm long pieces with one side lapped and chamfered and the other side polished to a root mean square (RMS) surface roughness of less than 50 nm.

Preparation of substrates for in situ X-ray absorption spectroscopy (XAS) characterization: Electrode substrates for in situ XAS characterization were prepared from 200 mm long GC rods (diameter 10 mm, Sigradur G HTW Hochtemperatur-Werkstoffe GmbH). Before deposition of MnO or Au nanoparticles, the rods were processed by the Stanford crystal shop to produce ca. 100−200 μm thick wafers with one side lapped and the other side polished to a surface RMS roughness of less than 50 nm.

Synthesis of catalyst materials: MnO nanoparticles were prepared with a sputtering system (Nanosys500, Mantis Deposition Ltd.) using a glow discharge magnetron sputtering with an inert gas condensation technique,[24,25] as described previously.[26] Briefly, the system consists of a nanoparticle source and the quadrupole mass filter, which filters sputtered nanoparticles by mass in situ. An elemental manganese target was used to sputter Mn nanoparticles. Mn nanoparticles were size selected at approximately 10 nm and deposited at a pressure of 0.3 mTorr with a rate of 0.16 Å·s^{-1}, monitored by a quartz crystal microbalance (QCM). These size selected nanoparticles were channeled to the main chamber and deposited on substrates. After deposition, samples were transferred to the load lock chamber, which was vented with Ar. The surface of the nanoparticles oxidized upon exposure to air. Gold nanoparticles were prepared using an electron beam evaporator to deposit 8 Å gold at a rate of 0.1−0.2 Å·s^{-1} monitored by a QCM.

Electrochemical characterization: The OER activity of the catalyst samples was characterized using cyclic voltammetry in a three electrode electrochemical cell in a rotating disk electrode (RDE) configuration. Characterization was performed in 0.1 M KOH electrolyte using a scan rate of 20 mV·s^{-1}, at room temperature. A carbon rod (Ted Pella) was used as the counter electrode, while Ag|AgCl (Fisher Scientific) was used as the reference electrode. The potential scale was calibrated to a reversible hydrogen electrode (RHE), and all the potentials were *iR*-compensated to 85% and reported vs RHE. The average measured resistance between the working and reference electrodes was ∼40 Ω for all samples. The OER activity was determined by scanning the potential from 0.05 V to 1.7−1.8 V in a N_2 saturated environment. To prepare surfaces for ex situ XAS characterization, the potential was scanned from 0.05 V to a vertex potential of 1.65 V at 20 mV·s^{-1} and held at 1.65 V for 30 min.

Physical and chemical characterization of nanoparticles: The size and morphology of the catalytic materials were investigated using scanning electron microscopy (SEM, FEI Magellan 400XHR). The images were obtained using a secondary electron detector, a beam current of 25 pA, and beam voltage of 5 kV. The oxidation state of the MnO_x nanoparticles was characterized using ex situ and in situ X-ray absorption spectroscopy (XAS) at Stanford Synchrotron Radiation Lightsource (SSRL).

Ex situ measurements were performed on the 31-pole wiggler beamline 10−1 at the SSRL using a ring current of 350 mA and a 1000 L·mm^{-1} spherical grating monochromator with 40 μm entrance and exit slits, providing ∼10^{11} ph·s^{-1} at 0.3 eV resolution in a 1 mm^2 beam spot. All data were acquired in a single load at room temperature and under ultrahigh vacuum (10^{-9} Torr) in total or auger electron yield (TEY, AEY) modes. The measurements were performed on MnO_x nanoparticles and five powder standards (MnF_2, MnO, Mn_3O_4, Mn_2O_3, and α-MnO_2) attached to an aluminum sample holder using conductive carbon. α-MnO_2 powder was prepared by dissolving 0.5 g of $KMnO_4$ in 30 mL of Millipore water, followed by dropwise addition of ethanol under stirring, drying the resulting powder at 60 °C overnight, and calcining the powder at 400 °C for 3 h. MnF_2, MnO, Mn_3O_4, and Mn_2O_3 powders were purchased from Sigma-Aldrich and used as received. The energy was carefully calibrated in two steps, by first correcting the energy scale for the drift in the beam energy and then aligning the energy of the first peak of the Mn_3O_4 powder control with a literature value of 639.6 eV.[27] Normalization details are described in the Supporting Information.

In situ hard X-ray XAS measurements were carried out at the SSRL at beamline 6-2 ES2. The beamline was operated with a double-crystal Si(311) monochromator with a Rh-coated mirror to reject the high order harmonics. The X-ray beam was focused with a parabolic mirror to a spot size of 230 μm fwhm (V) by 400 μm fwhm (H) at the sample position. The X-ray energy was calibrated to the pre-edge absorption peak (6543.3 eV) of potassium permanganate. The Mn Kα1 signals were resolved by 6 spherically bent analyzer crystals Ge ⟨333⟩ installed on the high energy resolution X-ray emission spectrometer[28] and detected by a silicon drift detector in photon counting mode. Multiple scans were collected at different sample positions at the potentials of interest. All spectra were normalized to have an edge jump of unity after linear backgrounds were subtracted from the raw data. The error bars reported in the spectra and the residuals represent one standard deviation based on Poisson statistics and standard error propagation.

In situ electrochemical characterization was performed in a similar setup as reported previously.[29] Completely separate electrochemical cells (custom built cells, Adams & Chittenden), reference electrodes (Ag|AgCl, BASi), and counter electrodes (100 mm length/5 mm diameter glassy carbon rod, Si gradur G HTW Hochtemperatur-Werkstoffe GmbH) were used with the MnO-GC and MnO/Au-GC samples to avoid the possibility of contaminating the MnO-GC sample with trace amounts of Au. The working electrodes (GC wafers with deposited nanoparticulate catalysts) were glued to the window of the electrochemical cell using epoxy. The schematic of the in situ electrochemical cell is shown in Supporting Information, Figure S1. Prior to performing XAS measurements, cyclic voltammograms were collected at 20 mV·s^{-1} in nitrogen-saturated 0.1 M KOH electrolyte by first scanning the potential from 0.05 to 1.1 V and then from 0.05 to 1.65 V. To record in situ Mn XANES spectra at an OER relevant potential, the potential was scanned from 0.05 V to a vertex potential of 1.65 V at 20 mV·s^{-1} and held at 1.65 V for 15 min. All measurements were *iR*-compensated to 85% and are reported vs RHE by assuming a potential shift of 0.960 V. The average measured resistance between the working and the reference electrodes was ∼70 Ω.

Effect of Au: To further study the effect of Au on the OER activity of MnO-GC nanoparticles, additional electrochemical experiments were carried out. For these experiments, the potential was scanned on a MnO sample and bare GC support from 0.05 V to 1.8 V in a N_2 saturated environment. Then 0.1 mM $HAu(III)Cl_4$ hydrate (Sigma Aldrich, 99.999% metals basis) was added to each electrolyte and the samples were repeatedly scanned starting in the OER region, 1.2 to 1.8 V, with the cathodic scan progressively reaching more reductive potentials with each cycle to deposit increasing amounts of Au on the surface of the catalyst.

RESULTS AND DISCUSSION

Because the influence of the underlying substrate on the OER activity of MnO_x has not yet been clearly established in literature, we prepared nanoparticulate catalysts on inert GC supports to directly evaluate the impact of Au. These nanoparticulate catalysts consisted of sputtered MnO catalysts[26] and evaporated Au catalysts. The first sample consisted of only MnO deposited on GC (MnO-GC). The second and third samples consisted of both MnO and Au nanoparticles: one sample with MnO sputtered on top of Au nanoparticles evaporated onto GC (MnO/Au-GC), while in the other Au was evaporated on top of the MnO-GC catalyst (Au/MnO-GC).

Schematic representations and SEM images of the MnO-GC, MnO/Au-GC, and Au/MnO-GC catalysts are shown in Figure

dx.doi.org/10.1021/ja407581w | J. Am. Chem. Soc. 2014, 136, 4920−4926

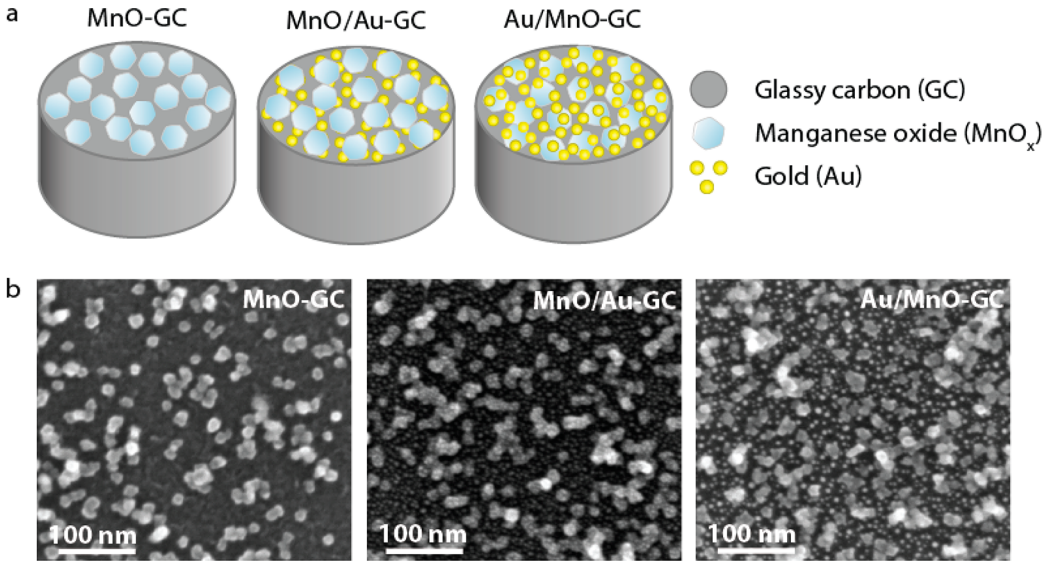

Figure 1. Schematic (a) and SEM images (b) of the three catalytic samples, MnO-GC, MnO/Au-GC, and Au/MnO-GC, illustrating morphology and coverage of glassy carbon support by MnO and Au nanoparticles.

1a,b. From the images, we can estimate that the MnO loading is less than 1 μg (calculations are presented in the Supporting Information). Total electron yield (TEY) Mn L-edge XAS characterization of the Mn surface oxidation state in the three catalysts is presented in Figure 2. In the figure, the XAS spectra

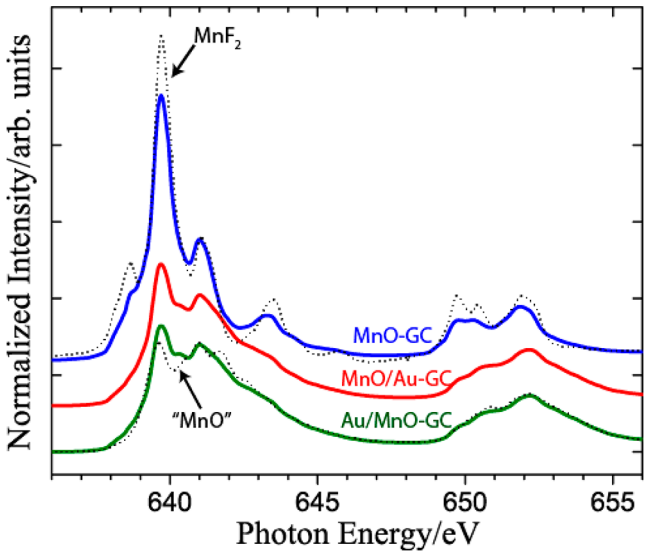

Figure 2. Total electron yield of Mn L-edge XAS of the three catalytic samples, MnO-GC, MnO/Au-GC, and Au/MnO-GC, and two powder standards, MnF2 and MnO. The surface of MnO, which is known to oxidize in air, was not sputtered prior to characterization and represents oxidized "MnO".

of the composite samples consisting of both MnO and Au are compared to the spectra of MnO-GC and two powder controls: MnF_2 and MnO. In these experiments, MnF_2 was used as a Mn^{II} powder standard in addition to commercially purchased MnO powder because of the known surface oxidation of the MnO phase in air.[27,30] Comparison of the spectra of the powder standards to the spectra of the as-deposited MnO/Au-GC and Au/MnO-GC catalysts using this surface-sensitive technique illustrates that after the addition of Au, MnO nanoparticles exhibit the oxidized form rather than the reduced form of the Mn^{II} phase. It is not clear whether this slight difference in the starting surface oxidation state results in a change in the crystal structure of the material to form a different bulk phase. Our attempts to characterize the crystallinity of the catalysts with and without the addition of Au using conventional and synchrotron grazing incidence X-ray diffraction (XRD) yielded only reflections corresponding to the GC support (Supporting Information, Figures S2 and S3). This indicated that either both types of samples were amorphous or that the crystallinity of the nanoparticles could not be detected using grazing incidence XRD.

Electrochemical characterization of the catalysts in 0.1 M KOH electrolyte shown in Figure 3 demonstrates that the composite catalysts, consisting of both MnO and Au nanoparticles, have significant OER activity, while the OER current density of the MnO-GC catalyst is negligible by comparison.

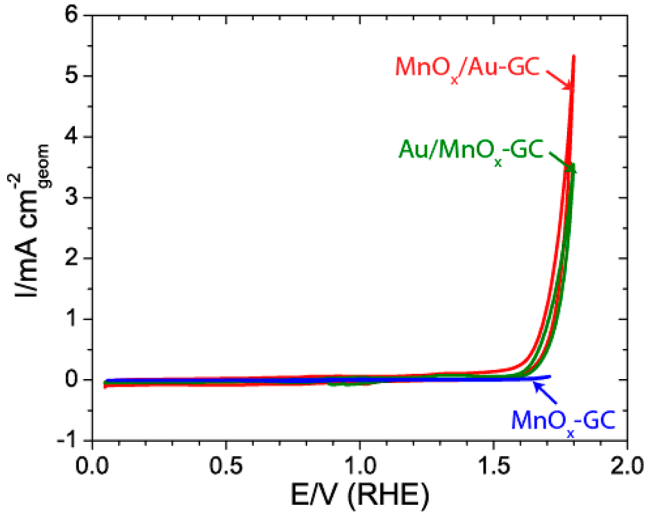

Figure 3. Cyclic voltammetry characterization of the three catalytic samples, MnO-GC, MnO/Au-GC, and Au/MnO-GC. Characterization was performed in 0.1 M KOH electrolyte, at 20 mV/s, and 1600 rpm.

dx.doi.org/10.1021/ja407581w | J. Am. Chem. Soc. 2014, 136, 4920−4926

Table 1. OER Activities of MnO_x Electrocatalysts at η = 300 and 400 mV

catalyst material/ type (author)	$I_{\eta=300}$ mA·cm$^{-2}_{geo}$	$I_{\eta=300}$ A·g^{-1} (est.)[a]	TOF$_{\eta=300}$ s^{-1} (est.)[b]	$I_{\eta\geq400}$ mA·cm$^{-2}_{geo}$	$I_{\eta\geq400}$ A·g^{-1} (est.)[a]	TOF$_{\eta\geq400}$ s^{-1} (est.)[b]
MnO/Au-GC (this work)	0.09	100	0.01	0.23	200	0.03
Au/MnO-GC (this work)	0.04	30	0.006	0.14	100	0.02
MnO-GC (this work)	0.007	6	0.001	0.04	10	0.002
β-MnO_2-α-Mn_2O_3 (Morita[7])	N/A	N/A	N/A	10	10	0.003
γ-MnOOH/Au (El-deab[22])	N/A	N/A	N/A	3	N/A	N/A
α-Mn_2O_3 (Gorlin[10])	1	6	0.002	2.34	10	0.006
MnO-ALD (Pickrahn[31])	0.4	20	0.003	0.61	30	0.005
MnOOH/Pt(111) (Subbaraman[6])	N/A	N/A	N/A	N/A	N/A	N/A
MnO_x (Trotochaud[20])	0.002	2	0.0004	N/A	N/A	N/A
β-MnO_2 (Fekete[13c])	N/A	N/A	N/A	6	0.4	0.0001

[a]Details of the calculations are presented in the Supporting Information. [b]Details of the calculations. [c]The authors report TOF for η = 600 mV.

The Supporting Information (Figure S4) also presents characterization of Au evaporated onto GC in the absence of MnO (Au-GC) to rule out simple additive effects of MnO-GC and Au-GC. From the inset in Figure S4 it is clear that the OER current of the composite samples is significantly greater than the sum of the individual activities of MnO-GC and Au-GC.

Table 1 compares the OER activity metrics of MnO-GC, MnO/Au-GC, and Au/MnO-GC, including geometric current density, mass activity, and turnover frequency (TOF), all calculated at either 300 or 400 mV overpotential (η), to the activity metrics of some of the best MnO_x electrocatalysts reported in literature.[6,7,10,13,20,31] Although Table 1 focuses purely on electrocatalysts, Supporting Information, Table S1 presents a similar comparison to exceptional manganese oxide photochemical water oxidation catalysts. The tabulated activity metrics for manganese oxide catalysts reveal that the catalytic behavior of MnO-GC in the absence of Au is consistent with expectations. Although its current density normalized to the geometric surface area is low in magnitude, the mass activity and TOF values of the catalyst match the performance of the best MnO_x OER catalysts. Furthermore, normalization of MnO-GC OER current by its capacitance produces similar surface-area normalized activity to that of the previously reported MnO thin film catalyst (Supporting Information, Figure S6) deposited by atomic layer deposition (ALD).[31]

From Tables 1 and S1, it is also apparent the two composite catalysts consisting of both MnO and Au nanoparticles exhibit unusually high OER activities. Each mass activity and TOF is about an order of magnitude higher than the corresponding metrics for the previously reported highly active thin film MnO_x catalysts. The only other MnO_x catalyst with similar activity was published by Subbaraman and co-workers, who electro-deposited MnO_x islands on a Pt(111) support. Although the authors did not include a CV of MnO_x demonstrating its OER activity, they reported an OER current (on a geometric basis) of 5 mA·cm^{-2} at ca. η = 560 (1.78 V). This geometric current density is similar to the geometric current densities of our composite catalysts after the background OER current of Pt(111) substrate is subtracted. From the results of Subbaraman and co-workers, it is not clear whether or not the use of a noble metal support has an impact on the measured OER activity of MnO_x catalyst. Direct comparison between the activity metrics of MnO-GC and Au/MnO-GC catalysts in the present report, however, convincingly demonstrates that the addition of a noble metal to MnO nanoparticles sputtered onto a GC substrate will lead to a significant enhancement in their OER activity.

The influence of adding Au to the OER activity of MnO_x could occur either through a modification of the MnO phase of the starting catalyst, thus creating a bulk MnO_x phase with intrinsically higher OER activity than the original catalyst, or through the formation of active sites at the interface of MnO_x and Au. To probe this further, we characterized the catalytic surface after exposure to OER conditions. In Figure 4, we present ex situ TEY Mn L-edge XAS spectra of MnO-GC, MnO/Au-GC, and Au/MnO-GC catalysts previously exposed to an OER relevant potential of 1.65 V. The corresponding chronoamperometry curves used to generate the OER catalytic surfaces are shown in Supporting Information, Figure S7. As expected, exposure to oxidative potentials leads to oxidation of MnO nanoparticles in all three cases. The presence of Au, however, favors formation of less oxidized MnO_x nanoparticles. Furthermore, in the Au/MnO_x-GC catalyst where Au is deposited on top of the MnO nanoparticles, Mn assumes the lowest oxidation state among the three OER samples (Supporting Information, Figure S8). One potential explanation for this result is that after exposure to OER conditions, the Mn oxidation state may vary as a function of a distance from Au, with MnO_x located at the interface with Au assuming a more reduced state than MnO_x located away from Au.

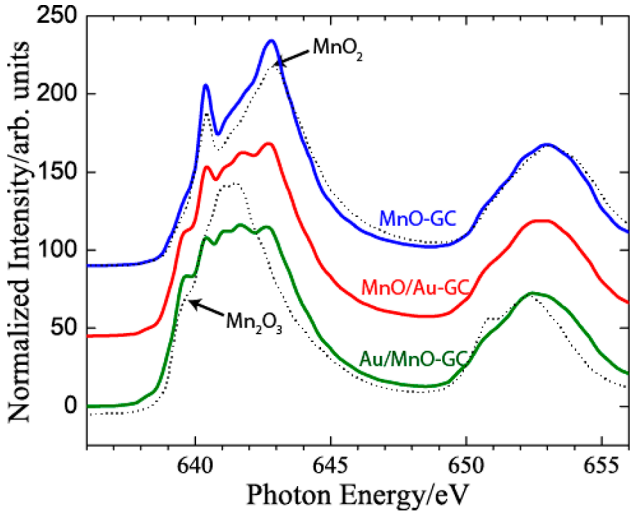

Figure 4. Total electron yield Mn L-edge XAS of the three catalytic samples, MnO-GC, MnO/Au-GC, and Au/MnO-GC, and two powder standards, MnO_2 and Mn_2O_3.

To further study the possible interface effect in the composite samples, we compared Mn L-edge XAS spectra of

dx.doi.org/10.1021/ja407581w | J. Am. Chem. Soc. 2014, 136, 4920−4926

MnO/Au-GC and MnO-GC samples in TEY and auger electron yield (AEY) detection modes. Although both AEY and TEY detection modes are surface sensitive, the probing depth of AEY is shallower than that of TEY.[27] If an interface effect is present, one would expect the measured oxidation state of the oxidized MnO_x nanoparticles in the MnO/Au-GC sample to vary as a function of probe depth[32] as illustrated in the schematic in Supporting Information, Figure S9, resulting in different TEY and AEY spectra. Figure S9 also presents the AEY and the TEY spectra of MnO-GC and MnO/Au-GC for the as-deposited and for the OER samples. Comparison of AEY and TEY spectra of MnO_x in the absence of Au (the MnO-GC sample) in Figure S9 demonstrates a lack of variation in Mn oxidation state as a function of distance from the GC support, both before and after applying an OER relevant potential. Making the same comparisons with the MnO/Au-GC sample, however, shows that while the as-deposited sample has a negligible difference in the Mn spectra between AEY and TEY mode, a more significant spectral difference is observed for the sample exposed to OER relevant potentials. In that sample, the top of the nanoparticle, which is located away from the Au-MnO_x interface, is likely more oxidized, resembling the spectra of the MnO-GC sample exposed to OER conditions. These results support the hypothesis that there is an interface effect between Au and MnO_x after MnO is exposed to high oxidative potentials. In conventional heterogeneous catalysis, such an interface effect has been previously observed with MnO_2[33] and other reducible metal oxides, such as TiO_2[34] and Ce_2O_3,[34,35] in contact with Au. The ex situ nature of the Mn L-edge XAS characterization, however, does not allow us to differentiate between an interface effect that emerges when the catalyst is under OER conditions or an interface effect that emerges after the catalyst is removed from the electrochemical cell. To answer this question, in situ methods were required.

In situ characterization was performed with a bulk-sensitive technique using Mn K-edge XAS. Our measurements focused on the X-ray absorption near edge structure (XANES) region, which probes the bulk electronic structure of the catalyst. In the experiments, MnO and Au nanoparticles were deposited on ~200 μm thick GC wafers to allow X-ray illumination of the backside of the electrodes. We characterized two samples, MnO-GC and MnO/Au-GC, with a slightly reduced loading of MnO compared to the ex situ samples (Supporting Information, Figure S10). These samples were held at 1.65 V during the Mn K-edge XAS measurement. Despite the MnO/Au-GC sample having a higher OER current throughout the entire experiment (Figure S10), our in situ XAS characterization shown in Figure 5 does not reveal a measurable difference between the XANES spectra of Mn in the MnO-GC and the MnO/Au-GC samples. The observation of the same average Mn oxidation during the electrochemical evolution of oxygen for both samples suggests that a small subset of sites rather than the bulk phase is critical to the enhanced OER catalysis in the samples containing Au nanoparticles; for example, this could occur by means of some of the MnO_x sites locally interacting with Au in such a way as to form OER active sites with modified properties during electrochemical characterization.

To further explore this hypothesis we performed electrochemical characterization of the MnO-GC catalyst before and after adding 0.1 mM of $HAu(III)Cl_4$ to the electrolyte. Figure 6 shows that as we electrodeposit more Au onto the surface by sweeping to more reductive potentials, the OER activity

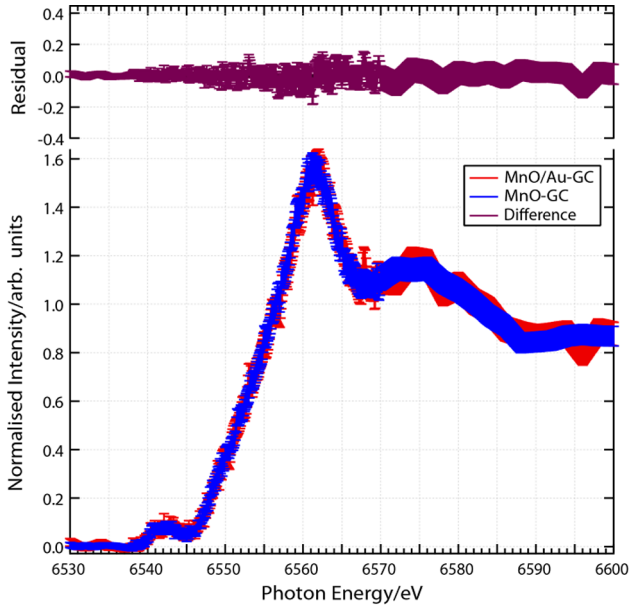

Figure 5. Mn K-edge XAS of two catalytic samples, MnO-GC and MnO/Au-GC, and the difference between the two spectra, demonstrating that Mn has a similar oxidation state under OER conditions in the presence and absence of Au.

increases, eventually reaching a current density greater than 10 $mA{\cdot}cm^{-2}$ at 1.8 V. When the same experiment was performed with a bare GC substrate, we also observed an increase in the OER activity with increased electrodeposition of Au, but the activity remained low, below 1 $mA{\cdot}cm^{-2}$ at 1.8 V. These experiments demonstrate that the addition of Au salt to the characterization electrolyte will lead to a similar enhancement in OER activity of MnO-GC catalyst as evaporation of Au onto the catalytic surface prior to electrochemical characterization. Some dissolution of Au into electrolyte is expected to occur at the highly oxidative potentials necessary for the OER.[36] We took advantage of this fact and also performed experiments with the MnO-GC sample in the setup previously used to characterize samples containing evaporated Au nanoparticles, but without cleaning the cell. Thus, trace Au was expected to be present to form a sample which we refer to as "trace-Au/MnO-GC". Supporting Information, Figure S11 shows that although the morphology of the MnO nanoparticles in trace-Au/MnO-GC had not changed while evaluating OER activity, the OER current increased with time during a potential hold at 1.65 V for 30 min (after first cycling the catalyst from 0.05 to 1.65 V at 20 $mV{\cdot}s^{-1}$), ultimately rising to the same level of OER activity as that for the Au/MnO-GC sample. This result further illustrates that the electrolyte conditions can have a significant effect on the activity of MnO_x, with the addition of only a trace amount of Au leading to a significant increase in the OER activity.

Supporting Information, Figure S12 compares cyclic voltammograms of the Au-GC, Au/MnO-GC, and trace-Au/MnO-GC samples. Analysis of electrochemical features of the samples confirms the presence of Au in trace-Au/MnO-GC sample and reveals that the presence of MnO_x has an influence on the red-ox properties of Au. Specifically, the addition of MnO_x leads to formation of multiple oxidation/reduction peaks as opposed to the one clear oxidation peak and the one clear reduction peak observed in the Au-GC sample. The presence of multiple oxidation/reduction peaks in both Au/MnO-GC and

dx.doi.org/10.1021/ja407581w | J. Am. Chem. Soc. 2014, 136, 4920−4926

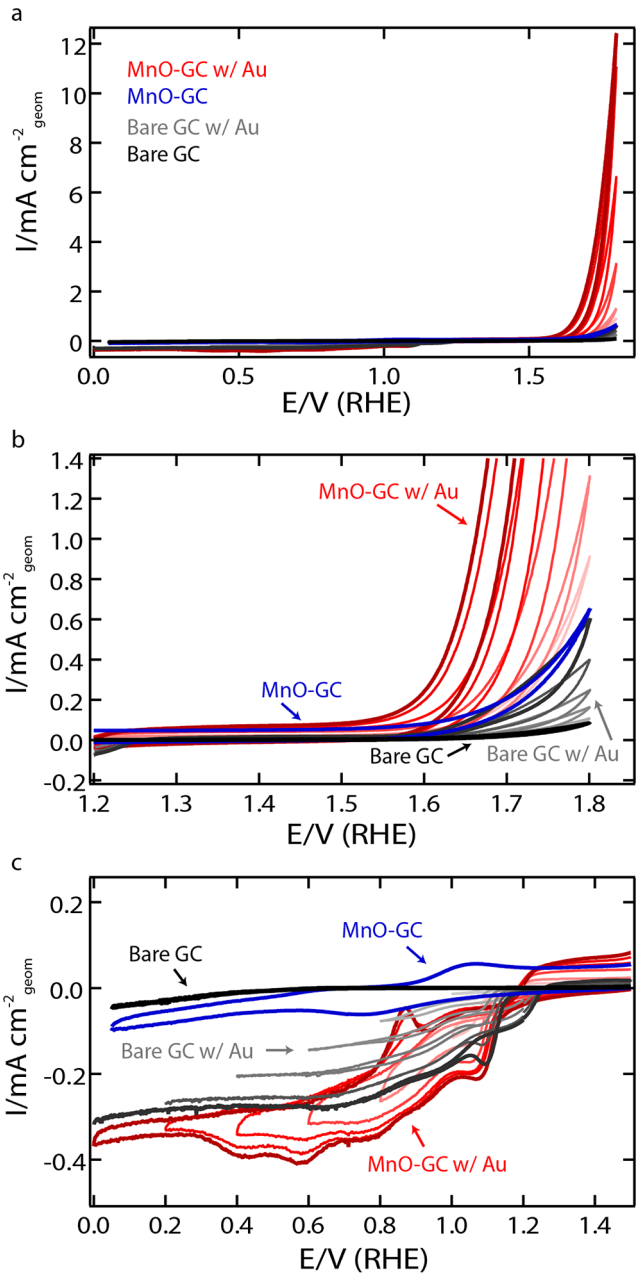

Figure 6. (a) Cyclic voltammetry of MnO-GC and bare GC support in the presence and absence of trace amount of Au (0.1 mM $HAu(III)Cl_4$) demonstrating the increasing OER activity with increasing deposition of Au; (b) 10-fold magnification of panel a focusing on the OER region. (c) 100-fold magnification of panel a focusing on the reductive region.

trace-Au/MnO-GC could indicate that the interactions between Au and MnO_x have led to a formation of Au sites with different strengths of Au−OH adsorption. Since reducible metal oxides such as MnO_2 are known to interact with noble metals to form a more oxidized noble metal at the interface of the two materials,[37] this result is consistent the presence of interfacial effects between MnO_x and Au.

After taking into account our ex situ and in situ spectroscopic characterization as well as electrochemical studies, we propose that the observed enhancement in the OER activity of MnO_x in the presence of Au is caused by the local participation of Au in the OER catalysis, for example through dissolution of Au and its re-deposition onto a subset of MnO_x sites, rather than a bulk change in the starting properties of MnO_x. This interpretation is consistent with all of the results in our study and is also supported by the published literature in the area of OER catalysis for bulk MnO_x materials. As described previously, Table 1 convincingly demonstrates that the samples consisting of both MnO_x and Au had anomalously high OER activity when compared to other active MnO_x OER catalysts. The only MnO_x catalyst that had been reported to have similar OER activity was a manganese oxyhydroxide prepared using a completely different method, an electrodeposition, but also in the presence of a noble metal, Pt(111).[6] Similar to Au, Pt is known to interact with transition metal oxides to form a reduced oxide and an oxidized metal at the interface of the two materials[37,38] and dissolve at oxidizing potentials relevant to the OER.[36] Therefore, the presence of Pt during the OER could lead to an enhancement in the OER activity of MnO_x that is similar to the enhancement observed in the presence of Au. Additionally, a recent work from Najafpour and Sedigh reports that several of MnO_x phases, including Mn_3O_4, α-Mn_2O_3, β-MnO_2, and K-birnessite can convert to the same layered MnO_x structure under water oxidizing conditions.[39] As discussed by the authors, this observation deemphasizes the nature of the starting MnO_x phase in the OER catalysis and highlights the importance of the electrolyte conditions during water oxidation.[39] Therefore, the presence of a noble metal in the catalyst sample or the electrolyte could have a greater influence on the formation of the OER active sites than the as-deposited phase of MnO_x.

The effect of electrolyte conditions on the OER activity of electrocatalysts is not limited to MnO_x. Trotochaud and co-workers have recently reported transformation of NiO_x thin film catalyst into a layered hydroxide/oxyhydroxide OER catalyst during electrochemical characterization.[20] During the transformation, the catalyst scavenged Fe impurities from the solution incorporating them into the final active catalytic structure.[20] It is possible that like MnO_x, NiO_x could also interact with noble metal additives to form OER active sites with enhanced TOFs. For example, in a different study, Yeo and co-workers have already demonstrated a higher TOF with a catalyst consisting of only 0.14 monolayers of NiO_x deposited on Au relative to the TOF of a bulk NiO_x catalyst, indicating that an interaction between NiO_x and Au exists.[21] Although Trotochaud and co-workers have also attempted to assess the role of Au by characterizing NiO_x catalysts on Au/Ti and ITO supports, their study involved conformal NiO_x thin films with limited electrochemical accessibility of the Au support.[20] In contrast, in the study by Yeo and co-workers, the Au oxidation/reduction features were still present in the submonolayer sample, which meant that Au had an opportunity to locally impart OER activity by either interacting with the adjacent NiO_x or by dissolving into the electrolyte at the high oxidizing potentials necessary for the OER[36] and subsequently integrating into the NiO_x catalyst. Thus, the electrochemical accessibility of the Au likely plays a role and should be an important consideration when designing catalyst morphologies for future studies.

CONCLUSIONS

In an investigation of catalysts for the oxygen evolution reaction (OER), we have shown that a composite catalyst of MnO nanoparticles in the presence of Au exhibited an enhancement in electrocatalytic activity by 1 order of magnitude over the best

dx.doi.org/10.1021/ja407581w | J. Am. Chem. Soc. 2014, 136, 4920−4926

reported pure MnO_x catalysts. A difference in the Mn L-edge X-ray absorption spectra of as-deposited catalysts originally indicated that a change in the starting properties of MnO_x could be responsible for the observed increase in the OER current. However, subsequent electrochemical measurements as well as ex situ and in situ Mn XAS characterization of the OER relevant samples identified more likely possibilities: namely local, interfacial effects between the Au and MnO_x. Even trace amounts of Au were sufficient to activate the catalyst for the OER, further indicating that a local interaction between Au and MnO_x, impacting only a subset of MnO_x sites, is the likely cause of the observed OER enhancement. As the intrinsic OER activity of other nonprecious metal oxides such as CoO_x and NiO_x (Supporting Information, Table S2)[6,17,21] are even higher than that of MnO_x, investigating the role of Au in the OER activities of a number of nonprecious metal-based transition metal oxide catalysts could lead to even higher-performance materials.

■ ASSOCIATED CONTENT

Supporting Information

Figures and tables as described in the text; details on X-ray absorption spectra normalization; details on the calculations of the OER activity metrics. This material is available free of charge via the Internet at http://pubs.acs.org.

■ AUTHOR INFORMATION

Corresponding Author

jaramillo@stanford.edu

Notes

The authors declare no competing financial interest.

■ ACKNOWLEDGMENTS

This study was supported as part of the Center on Nanostructuring for Efficient Energy Conversion (CNEEC) at Stanford University, an Energy Frontier Research Center funded by the U.S. Department of Energy, Office of Science, Office of Basic Energy Sciences under Award No. DE-SC0001060. SEM and conventional XRD characterization were performed at the Stanford Nanocharacterization Laboratory part of the Stanford Nano Shared Facilities. XAS and synchrotron XRD characterizations were carried out at the Stanford Synchrotron Radiation Lightsource, a Directorate of SLAC National Accelerator Laboratory and an Office of Science User Facility operated for the U.S. Department of Energy Office of Science by Stanford University. The SSRL Structural Molecular Biology Program is supported by the DOE Office of Biological and Environmental Research, and by the National Institutes of Health, National Center for Research Resources, Biomedical Technology Program (P41RR001209). The authors would like to thank Arturas Vailionis and Chad Miller for help with grazing incidence XRD measurements at SSRL, Monica Garcia Mota, Jens Nørskov, and Arnold Forman for helpful discussions and Sung-Hyeon Baeck for the synthesis of α-MnO_2 powder.

■ REFERENCES

(1) Yeager, E. *J. Mol. Catal.* **1986**, *38*, 5.
(2) Lewis, N. S.; Nocera, D. G. *Proc. Natl. Acad. Sci. U.S.A.* **2006**, *103*, 15729.
(3) Trasatti, S. *Electrochim. Acta* **1984**, *29*, 1503.
(4) Jiao, F.; Frei, H. *Angew. Chem., Int. Ed.* **2009**, *48*, 1841.
(5) Miles, M. H.; Kissel, G.; Lu, P. W. T.; Srinivasan, S. *J. Electrochem. Soc.* **1976**, *123*, 332.
(6) Subbaraman, R.; Tripkovic, D.; Chang, K. C.; Strmcnik, D.; Paulikas, A. P.; Hirunsit, P.; Chan, M.; Greeley, J.; Stamenkovic, V.; Markovic, N. M. *Nat. Mater.* **2012**, *11*, 550.
(7) Morita, M.; Iwakura, C.; Tamura, H. *Electrochim. Acta* **1977**, *22*, 325.
(8) Najafpour, M. M.; Ehrenberg, T.; Wiechen, M.; Kurz, P. *Angew. Chem., Int. Ed.* **2010**, *49*, 2233.
(9) Jiao, F.; Frei, H. *Chem. Commun.* **2010**, *46*, 2920.
(10) Gorlin, Y.; Jaramillo, T. F. *J. Am. Chem. Soc.* **2010**, *132*, 13612.
(11) Robinson, D. M.; Go, Y. B.; Greenblatt, M.; Dismukes, G. C. *J. Am. Chem. Soc.* **2010**, *132*, 11467.
(12) Boppana, V. B. R.; Jiao, F. *Chem. Commun.* **2011**, *47*, 8973.
(13) Fekete, M.; Hocking, R. K.; Chang, S. L. Y.; Italiano, C.; Patti, A. F.; Arena, F.; Spiccia, L. *Energy Environ. Sci.* **2013**, *6*, 2222.
(14) Man, I. C.; Su, H.-Y.; Calle-Vallejo, F.; Hansen, H. A.; Martínez, J. I.; Inoglu, N. G.; Kitchin, J.; Jaramillo, T. F.; Nørskov, J. K.; Rossmeisl, J. *ChemCatChem* **2011**, *3*, 1159.
(15) Brossard, L. *Int. J. Hydrogen Energy* **1992**, *17*, 671.
(16) Potvin, E.; Brossard, L. *J. Appl. Electrochem.* **1995**, *25*, 462.
(17) Yeo, B. S.; Bell, A. T. *J. Am. Chem. Soc.* **2011**, *133*, 5587.
(18) Kanan, M. W.; Nocera, D. G. *Science* **2008**, *321*, 1072.
(19) Gardner, G. P.; Go, Y. B.; Robinson, D. M.; Smith, P. F.; Hadermann, J.; Abakumov, A.; Greenblatt, M.; Dismukes, G. C. *Angew. Chem., Int. Ed.* **2012**, *51*, 1616.
(20) Trotochaud, L.; Ranney, J. K.; Williams, K. N.; Boettcher, S. W. *J. Am. Chem. Soc.* **2012**, *134*, 17253.
(21) Yeo, B. S.; Bell, A. T. *J. Phys. Chem. C* **2012**, *116*, 8394.
(22) El-Deab, M. S.; Awad, M. I.; Mohammad, A. M.; Ohsaka, T. *Electrochem. Commun.* **2007**, *9*, 2082.
(23) Mohammad, A. M.; Awad, M. I.; El-Deab, M. S.; Okajima, T.; Ohsaka, T. *Electrochim. Acta* **2008**, *53*, 4351.
(24) Yamada, I.; Usui, H.; Takagi, T. *Z. Phys. D* **1986**, *3*, 137.
(25) Ayesh, A. I.; Qamhieh, N.; Ghamlouche, H.; Thaker, S.; El-Shaer, M. *J. Appl. Phys.* **2010**, *107*, 034317.
(26) Gorlin, Y.; Chung, C.-J.; Nordlund, D.; Clemens, B. M.; Jaramillo, T. F. *ACS Catal.* **2012**, *2*, 2687.
(27) Gilbert, B.; Frazer, B. H.; Belz, A.; Conrad, P. G.; Nealson, K. H.; Haskel, D.; Lang, J. C.; Srajer, G.; De Stasio, G. *J. Phys. Chem. A* **2003**, *107*, 2839.
(28) Sokaras, D.; Weng, T.-C.; Nordlund, D.; Alonso-Mori, R.; Velikov, P.; Wenger, D.; Garachtchenko, A.; George, M.; Borzenets, V.; Johnson, B.; Rabedeau, T.; Bergmann, U. *Rev. Sci. Instrum.* **2013**, 84.
(29) Gorlin, Y.; Lassalle-Kaiser, B.; Benck, J. D.; Gul, S.; Webb, S. M.; Yachandra, V. K.; Yano, J.; Jaramillo, T. F. *J. Am. Chem. Soc.* **2013**, *135*, 8525.
(30) Qiao, R.; Chin, T.; Harris, S. J.; Yan, S.; Yang, W. *Curr. Appl. Phys.* **2013**, *13*, 544.
(31) Pickrahn, K. L.; Park, S. W.; Gorlin, Y.; Lee, H.-B.-R.; Jaramillo, T. F.; Bent, S. F. *Adv. Energy Mater.* **2012**, *2*, 1269.
(32) Regan, T. J.; Ohldag, H.; Stamm, C.; Nolting, F.; Lüning, J.; Stöhr, J.; White, R. L. *Phys. Rev. B* **2001**, *64*, 214422.
(33) Longo, A.; Liotta, L. F.; Carlo, G. D.; Giannici, F.; Venezia, A. M.; Martorana, A. *Chem. Mater.* **2010**, *22*, 3952.
(34) Rodriguez, J. A.; Ma, S.; Liu, P.; Hrbek, J.; Evans, J.; Pérez, M. *Science* **2007**, *318*, 1757.
(35) Baron, M.; Bondarchuk, O.; Stacchiola, D.; Shaikhutdinov, S.; Freund, H. J. *J. Phys. Chem. C* **2009**, *113*, 6042.
(36) Cherevko, S.; Topalov, A. A.; Zeradjanin, A. R.; Katsounaros, I.; Mayrhofer, K. J. J. *RSC Adv.* **2013**, *3*, 16516.
(37) Flytzani-Stephanopoulos, M.; Gates, B. C. *Annu. Rev. Chem. Biomol. Eng.* **2012**, *3*, 545.
(38) Fu, Q.; Wagner, T. *Surf. Sci. Rep.* **2007**, *62*, 431.
(39) Najafpour, M. M.; Sedigh, D. J. *Dalton Trans.* **2013**, *42*, 12173.